Letter

ADVANCED PHOTONICS

Optical analog of black and white gravitational holes

Eric Plum,[a,*] Anton N. Vetlugin,[b] Baurzhan Salimzhanov,[a] Nikolay I. Zheludev,[a,c] and Nina Vaidya[d,*]
[a]University of Southampton, Optoelectronics Research Centre and Centre for Photonic Metamaterials, Southampton, United Kingdom
[b]Nanyang Technological University, SPMS, TPI, Centre for Disruptive Photonic Technologies, Singapore
[c]Texas A&M University, Hagler Institute for Advanced Study, College Station, Texas, United States
[d]University of Southampton, Faculty of Engineering and Physical Sciences, Southampton, United Kingdom

Abstract. In general relativity, a gravitational "white hole" is a hypothetical region of space that cannot be entered from outside. It is the reverse of a "black hole" from which light and information cannot escape. We report an optical device exhibiting intriguing similarities to these objects. It will either totally absorb (optical black hole) or totally reject (optical white hole) light of any wavelength, depending on its polarization. The device's functionality is based on the formation of a standing wave from the wavefront of spatially coherent incident radiation. Interaction of the standing wave with a thin absorber enables coherent perfect absorption and transmission, whereas polarization sensitivity arises from the geometrical phase of the interfering beams. We provide experimental proof-of-principle demonstrations and show that the device operates as a black and white hole for orthogonal polarizations of the incident light. From a remote point, it will look similar to a gravitational black or white hole depending on the polarization of light. In principle, the optical black and white hole device can operate as a deterministic absorber or rejector throughout the entire electromagnetic spectrum. Broadband absorbers and rejectors can be useful for energy harvesting, detection, stealth technologies, and redistribution of light.

Keywords: coherent perfect absorption; temporal and spatial coherence; interference; absorption; reflection; geometric phase.

Received Oct. 18, 2024; revised manuscript received Dec. 23, 2024; accepted for publication Jan. 20, 2025; published online Feb. 27, 2025.

[DOI: 10.1117/1.AP.7.2.025001]

1 Introduction

All light that enters a gravitational singularity known as a black hole will never escape, whereas all light that tries to enter a white hole is rejected (Fig. 1). The fascinating electromagnetic properties of these objects have motivated the study of systems exhibiting similar characteristics from fluid dynamics,[1] acoustics,[2] and Bose–Einstein condensates[3] to linear[4,5] and nonlinear[6–9] optics. In particular, the previously proposed linear optical black holes have relied on metamaterials to imitate curved space–time with a complex refractive index profile.[4,5]

Here, we introduce the concept and provide a proof-of-principle demonstration of an "optical black and white hole" that deterministically absorbs all light of one linear polarization while rejecting all light of the orthogonal polarization. It relies on coherent perfect absorption[10] enabled by spatial coherence and interference; and has a simple geometry that can be implemented using available materials.

2 Perfect Absorption and Rejection through Interference

Although the effects of interference on absorption of a single beam of light have been studied for a long time,[11–15] only since 2012 it has become well known that interference of two coherent light beams on a thin absorber can eliminate the Joule losses of optical energy or, by contrast, can lead to total, deterministic absorption of light.[10,16,17]

Consider a thin light-absorbing film of subwavelength thickness. The result of interference of two temporally coherent counterpropagating incident beams of the same intensity on such a film is illustrated by two opposite cases. In the first, a

*Address all correspondence to Eric Plum, erp@orc.soton.ac.uk; Nina Vaidya, n.vaidya@soton.ac.uk

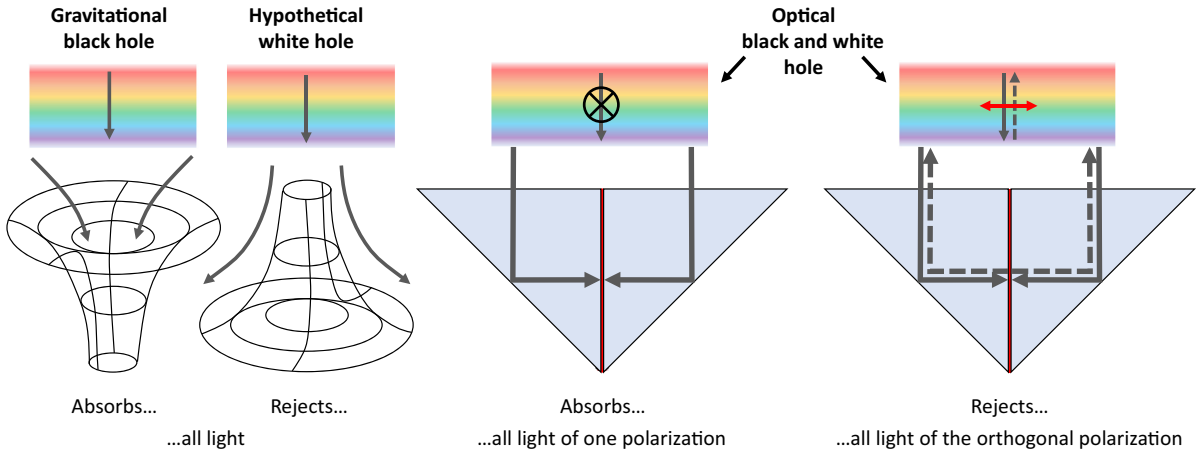

Fig. 1 Astronomical gravitational black holes swallow everything that crosses their event horizon. Their counterpart, the white hole, rejects everything, and it is hypothesized that its event horizon cannot be crossed from outside. The "optical black and white holes" absorb and reject all light depending on its polarization.

standing wave is formed with zero electric field, a node arising from destructive interference, at the position of the absorbing film. As the film is much thinner than the optical wavelength, its electric–dipole interaction with the electromagnetic field is negligible and the absorber will appear to be transparent for both incident waves. (The amplitude of the magnetic field is at a maximum here, but magnetic dipole transitions may be neglected in this simplified picture as they are typically much less efficient than electric dipole transitions.) In the second case, the film is at a position of constructive interference, an electric field maximum (antinode), where the electric–dipole interaction is strong and the associated absorption becomes very efficient.

Irrespective of the mechanism of absorption, an analysis of such interference[16] shows that perfect deterministic transmission and absorption of light can be achieved in a thin (relative to the wavelength) absorber if, for traveling-wave illumination, its reflectivity from either side is one-quarter, and one-half of optical power is absorbed in the film. For fundamental reasons, an infinitesimally thin film cannot absorb more than half of the energy from a traveling wave,[18,19] and a very close approximation of this limit is possible with natural materials (e.g., multilayered graphene[20] or thin metal layers[21–23]) or/and metamaterial structuring of films of nanoscale thicknesses.[10,24] If coherent waves of equal amplitude incident on both sides of such an absorber interfere constructively (or destructively) at the absorber, as described in the previous paragraph, then reflected and transmitted waves on either side of the absorber will have equal amplitude and a π (or 0) phase difference, resulting in complete cancellation (or constructive interference) of all outgoing fields and thus complete absorption (or transmission) of all incident light. In a bigger picture that includes the thermal radiation of the film, the Landsberg thermodynamic limit[25] caps the efficiency of radiative energy utilization at a value slightly lower than 100%.

The regime of nearly perfect absorption in a standing wave has been experimentally demonstrated with classical light,[10] single[26] and entangled photons,[27] and has been used in applications such as all-optical light modulation with ultrafast optical pulses,[28] single-photon optical switching,[29] data processing in classical[30] and quantum[31] networks, as well as image recognition.[32]

So far, we discussed perfect absorptivity and transmissivity arrangements involving two coherent counterpropagating beams. The interference required for perfect broadband absorption and transmission can be constructed by splitting an incident beam of light into two coherent beams using a beam splitter and directing these two beams to opposite sides of the absorber. However, this is not possible without a complex and bulky arrangement of multiple mirrors, making such absorbers impractical.

The main purpose of the present work is to demonstrate that interference on a thin absorber can lead to nearly perfect absorption of thermal or laser light from a broadband source utilizing its spatial coherence, i.e., uniformity of the phase of the wavefront. Spatial coherence is a characteristic feature of single-mode laser light but is also a feature of remote sources. Indeed, all waves are spatially coherent on sufficiently small-length scales.[33] For instance, light with wavelength $\lambda = 500$ nm that comes from the closest star outside the solar system, Proxima Centauri (star diameter $\delta = 214{,}550$ km), located at a distance $D = 4.25$ light-years from Earth is spatially coherent across a wavefront diameter of $d = 0.16\lambda D/\delta = 15$ m. Light from a similar star located within the Andromeda Galaxy, the closest major galaxy, at a distance of 2.54 million light-years, is spatially coherent across a wavefront diameter of 9000 km (e.g., the distance between the UK and Japan).

For the conceptual design that we propose in this work, consider two mirrors set at a right angle to each other and a thin absorber placed along the bisector plane separating them (Fig. 2). If the arrangement is narrower than the spatial coherence area of the incident radiation, light rays directed by the mirrors onto opposite sides of the same absorber area from nonoverlapping parts of the incident beam will be coherent and therefore interfere.

The type of interference is determined by the polarization of light. In the case of light that is linearly polarized in the plane of the absorber (perpendicular to the plane of incidence, i.e., *s*-polarization), the polarization state and relative phase of the

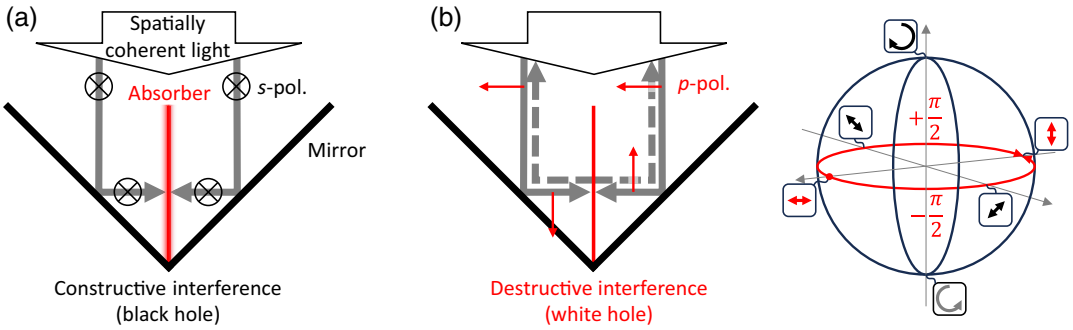

Fig. 2 Mechanism of complete absorption and complete rejection of light. Spatially coherent and normally incident (a) *s*-polarized light interferes constructively on a thin-film absorber placed at the bisector plane separating two mirrors set at a right angle to each other, resulting in coherent absorption, whereas (b) *p*-polarized light interferes destructively, resulting in coherent transmission, in principle with unlimited bandwidth. Destructive interference of incident *p*-polarized light occurs due to a geometric phase difference of π that arises from the rotation of the polarization state upon reflection, as illustrated on the Poincaré sphere. Constructive interference of incident *s*-polarized light is due to the absence of any polarization change and associated geometric phase.

waves propagating toward either side of the absorber do not change upon reflection: beams arriving on the opposite sides of the absorber are in phase and they interfere constructively [Fig. 2(a)]. Hence, this arrangement enables total absorption of any spectral component of the incident light: perfect broadband absorption.

However, if the incident light is polarized perpendicular to the plane of the absorber (parallel to the plane of incidence, i.e., *p*-polarization), upon reflection the electric-field vector rotates +90 deg on one of the mirrors and −90 deg on the other [Fig. 2(b)]. These polarization changes may be represented as trajectories between antipodal points on the Poincaré sphere, in opposite directions along its equator. With a sign depending on the direction of polarization rotation, the geometrical Pancharatnam–Berry phases[34] before and after reflection differ by an amount equal to half of the solid angle encompassed by their trajectory on the Poincaré sphere. Accordingly, the beams accrue a geometric phase difference of π upon reflection and interfere destructively at the absorber, resulting in electric-field cancellation and thus negligible absorption: a perfect arrangement for total transmission. Due to the geometric nature of the phase difference, the effect does not depend on the wavelength. Therefore, an incident light beam polarized perpendicular to the plane of the absorber will suffer no absorption for any spectral component, resulting in the reflection of all light by the device.

3 Experiment

The optical black and white hole device studied here consists of two identical 90-deg prisms manufactured from BK7 glass (Precision Optical Inc.) and polished to 80-nm surface flatness. The height of the prisms is 15 mm, whereas their legs are 21.3-mm wide. A 20-nm layer of chromium was deposited on a leg of one prism by thermal evaporation before the device was assembled by placing the chromium-coated prism face in contact with the uncoated prism, as shown in Fig. 1, with glass index-matching liquid covering the contact area to avoid any air gap, i.e., to ensure that the refractive index is the same on either side of the chromium film. For this proof-of-principle demonstration, the mirror reflections within the device occur by total internal reflection at the glass–air interfaces of the prism hypotenuses; we chose chromium as the absorber material, as it provides close to the desired absorption and reflection characteristics in a film of deep subwavelength thickness in the near-infrared part of the spectrum where the proof-of-principle demonstration is performed (S1.1, S1.2, and Fig. S6 in the Supplementary Material).

As illustrated by Fig. S7 in the Supplementary Material, the experiments were performed with the output of a continuous wave C + L band tunable laser (HP 8168F) with a spectral width of 100 kHz, which was collimated by a fiber collimator and directed toward the device such that the incident laser beam was centered on the boundary between the prisms. Reflected light then passed through an analyzer that selected one of the eigenpolarizations (*s* or *p*-polarization with the electric field parallel or perpendicular to the absorbing film) before being detected by an optical power meter. We measured the power r of the reflected light as a fraction of the incident optical power r_0 to determine the reflectivity of the device, $R_M = r/r_0$.

A small, fixed angle of incidence of $\beta \approx 2$ deg within the plane of the chromium film and a ∼1-mm slit were used to separate incident and reflected light, which had a Gaussian distribution with $1/e^2$ diameter of ∼7 mm in the plane perpendicular to the chromium film (Fig. S7 in the Supplementary Material). This spaces multiple reflections by more than the slit width, avoiding any additional interference or Fabry–Perot-cavity effects, allowing us to remove reflections from the glass–air interface analytically. To show the performance of antireflection–coated prisms, the 4% reflectivity of the glass–air interface has been removed from the measured reflectivity R_M, by calculating the reflectivity with an antireflection coating on the input face as $R = 1/\left(\frac{0.962}{R_M - 0.04} + 0.04\right)$. The absorptivity A is given by $A = 1 - R$. The optical paths were matched by translating one prism relative to the other using a piezo stage and optimizing the bandwidth of absorption for *s*-polarization, which also compensates for any slight size differences between the prisms of nominally identical size.

We investigated the dependence of reflectivity and absorptivity as functions of α (Fig. 3)—the beam's angle of incidence on the device—and laser wavelength λ (Fig. 4).

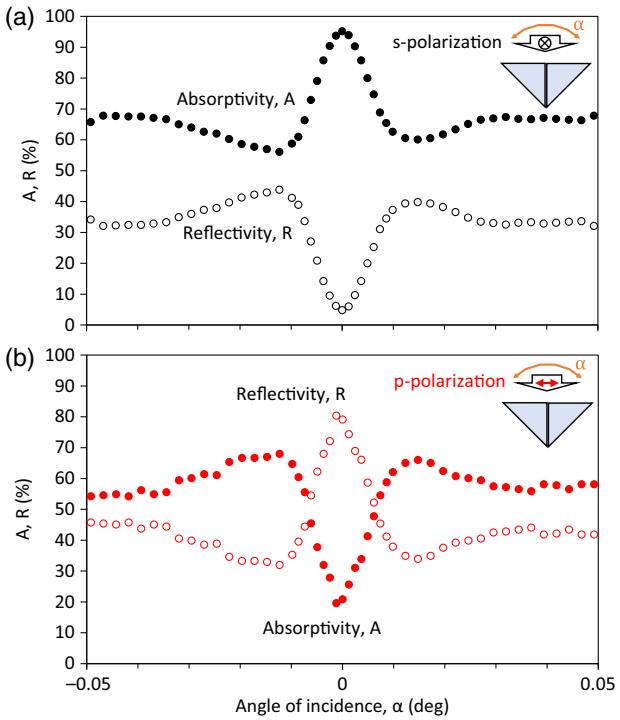

Fig. 3 Observation of the optical black and white hole analogs. Measured reflectivity and absorptivity of a chromium thin film on the interface between two identical glass prisms for (a) *s*- and (b) *p*-polarized light as a function of the angle of incidence. Absorption of *s*-polarized light (black hole) and rejection of *p*-polarized light (white hole) occur around normal incidence.

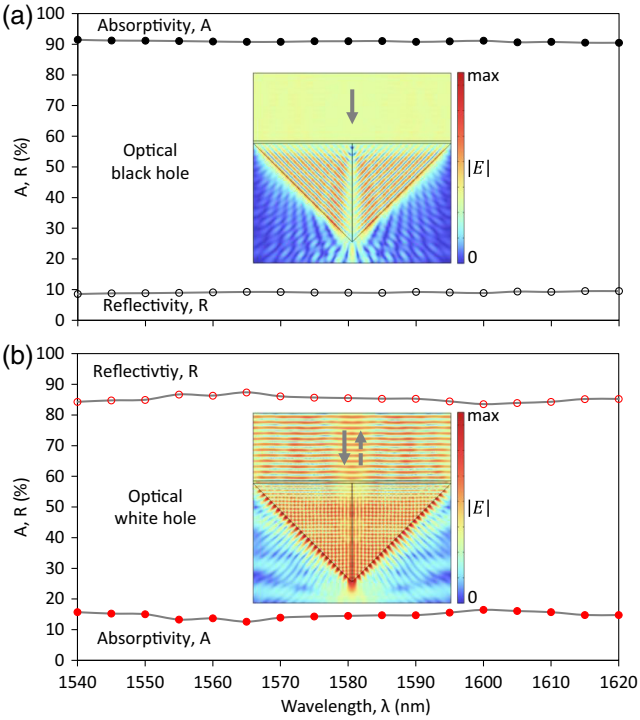

Fig. 4 Broadband absorption and rejection of light by optical (a) black and (b) white holes. Measured reflectivity and absorptivity as a function of wavelength at normal incidence. Inset simulations illustrate the absence of reflection from the device for the black hole case (a) and the formation of a standing wave due to interference of incident and reflected light for the white hole case (b).

Figure 3 shows the measured reflectivity and absorptivity at a wavelength of 1570 nm as a function of the angle of incidence for two incident polarizations (*s* and *p*) parallel and perpendicular to the plane of the absorbing film. At oblique incidence, a similar absorptivity of around 60% (~40% reflectivity) of the incident power is observed for both polarizations. However, as the angle of incidence approaches 0 deg, the absorptivity changes dramatically, approaching complete absorption (negligible rejection) for *s*-polarization and decreasing toward minimal absorption (increasing toward complete rejection) for *p*-polarization. Arguably, the rapid angular transition to black-hole-like absorption of *s*-polarized light and white-hole-like rejection of *p*-polarized light at normal incidence may be thought of as an event horizon.

Figure 4 shows the spectral dependence of the optical black and white hole responses. The observed reflectivity and absorptivity are spectrally flat across the tuning range of the laser, indicating that it is broadband. For the optical black hole case, we observe 91% absorption; however, we observed 85% reflectivity for the optical white hole case. Simulations illustrate traveling-wave propagation toward the device for the black hole case [Fig. 4(a)], where negligible interference above the prisms indicates the near-complete absence of reflected light. By contrast, for the white hole case [Fig. 4(b)], almost all light is rejected by the device, resulting in almost equal amplitudes of light propagating toward and away from the prisms and thus the formation of a standing wave. The simulations in Figs. 4(a) and 4(b) were carried out in COMSOL Multiphysics for *s*- and *p*-polarized coherent plane wave illumination ($\lambda = 1570$ nm, from the upper boundary) of aligned prisms with a leg length $L = 14$ μm and refractive index 1.5, with a 320-nm-thick antireflecting coating having a refractive index of 1.225 on the input face and with a 20-nm-thick absorber with a refractive index of $4.6 + 4.4i$. Lateral outer boundaries above the prisms are periodic, and a scattering condition was used for all other outer boundaries. (Light scattering from the prism tip becomes insignificant at macroscopic prism sizes and can also be avoided by adding a reflective coating; see S1.4 and Fig. S5 in the Supplementary Material.)

We note that the ultimately broadband optical black hole and white hole responses for *s*- and *p*-polarizations that occur for perfectly aligned identical prisms, can be reversed (over a large but finite bandwidth) by introducing a relative displacement $\Delta z = \lambda_0/2$ between the prisms, where λ_0 is the free-space wavelength and z is the direction of normal incidence (S1.3 in the Supplementary Material). The measurements in Fig. 4 illustrate this: they show *s*-polarization with $\Delta z \approx 0$ (black hole case) and $\Delta z \approx 800$ nm (white hole case). The tuning range of our laser is not large enough to distinguish between ideal and approximate black/white hole configurations.

4 Discussion

Although an ideal optical black and white hole is expected to deliver deterministic absorption and rejection of light, less than 100% absorptivity and reflectivity was observed in our proof-of-principle experiments. Causes of the finite absorptivity and

reflectivity include diffraction at edges and flatness of faces of the prisms, as well as wavefront distortions arising from imperfect illumination optics. Calculations show that various real absorber materials can deliver very close to deterministic absorption and deterministic rejection of light over multiple octaves of the electromagnetic spectrum (S1.2 in the Supplementary Material).

The acceptance angle within which near-complete absorption or rejection of light occurs as well as angular alignment tolerances is controlled by the size of the prisms and becomes large as the prism size L approaches the wavelength λ (S1.4 and Fig. S5 in the Supplementary Material). Arrays of microprism devices would offer large overall apertures and large acceptance angles, e.g., for light-harvesting applications, as well as large angular alignment tolerances. Translational alignment errors need to be small compared with the wavelengths of interest (S1.3 in the Supplementary Material), implying that larger translational errors relative to the prism size can be tolerated for smaller prisms and longer wavelengths.

In essence, ultimately broadband, complete absorption and rejection of light is a wave interference phenomenon enabled by a layer of substantial subwavelength thickness with suitable traveling-wave absorption and reflection characteristics. It follows that conceptionally similar black hole wave absorbers and/or white hole wave rejectors may be implemented for all sorts of waves. Indeed, coherent perfect absorption has been reported for electromagnetic waves from microwaves to optical frequencies[10–17] as well as for sound waves.[35–37] Although such works have demonstrated great potential, reliance on complex multicomponent interferometers has stood in the way of practical device implementations. By showing how spatial coherence can be exploited to achieve deterministic wave-matter interaction—or its deterministic absence—in simple, compact, monolithic, and broadband devices, the concept reported here indicates how the large body of work on thin-film coherent perfect absorption can be translated robustly into practical applications.

5 Conclusion

In summary, we have demonstrated how spatial coherence enables broadband deterministic absorption and rejection of light of orthogonal polarizations by simple and compact devices. We describe these as optical black and white holes, as the concept allows for complete absorption and rejection, in principle with unlimited bandwidth, characteristics shared with the black and white holes of general relativity. In practice, a very large bandwidth can be obtained, with limitations arising from the device size (Fig. S5 in the Supplementary Material) and material dispersion (S1.2 in the Supplementary Material). Our device implementation shows how the large body of work on coherent perfect absorption can be translated into practical devices, such as broadband energy harvesters, polarizers, perfect absorbers (e.g., for stealth technologies), and detectors. The latter could offer high quantum efficiency, directional selectivity, and sensitivity to spatial coherence and polarization. Arising from wave physics, the concept is also applicable to waves outside of electromagnetism, with implications from photonics to acoustics and beyond.

Disclosures

The authors declare no competing interests.

Code and Data Availability

The data shown in the figures are openly available from the University of Southampton ePrints research repository at https://doi.org/10.5258/SOTON/D2906.

Author Contributions

N.I.Z. suggested the double-prism arrangement of the absorption/rejection device. E.P. and N.V. designed the experimental setup and conducted the experiments. E.P. derived the analytical description. N.V. investigated black hole analogs and thermodynamic aspects. A.N.V. simulated and fabricated chromium films. B.S. conducted finite element method simulations. All authors analyzed the data and wrote and edited the paper.

Acknowledgments

This work is supported by the Zepler Institute Stimulus Fund, UK's Engineering and Physical Sciences Research Council (Grant Nos. EP/M009122/1 and EP/T02643X/1), and the Singapore National Research Foundation (Grant No. NRF2021-QEP2-01-P01).

References

1. S. Weinfurtner et al., "Measurement of stimulated Hawking emission in an analogue system," *Phys. Rev. Lett.* **106**(2), 021302 (2011).
2. M. Visser, "Acoustic black holes: horizons, ergospheres and Hawking radiation," *Class. Quantum Grav.* **15**(6), 1767 (1998).
3. J. R. Muñoz de Nova, K. Golubkov, and V. I. Kolobov, "Observation of thermal Hawking radiation and its temperature in an analogue black hole," *Nature* **569**(7758), 688–691 (2019).
4. D. A. Genov, S. Zhang, and X. Zhang, "Mimicking celestial mechanics in metamaterials," *Nat. Phys.* **5**(9), 687–692 (2009).
5. E. E. Narimanov and A. V. Kildishev, "Optical black hole: broadband omnidirectional light absorber," *Appl. Phys. Lett.* **95**(4), 041106 (2009).
6. T. G. Philbin et al., "Fiber-optical analog of the event horizon," *Science* **319**(5868), 1367–1370 (2008).
7. F. Belgiorno et al., "Hawking radiation from ultrashort laser pulse filaments," *Phys. Rev. Lett.* **105**(20), 203901 (2010).
8. R. A. Tinguely and A. P. Turner, "Optical analogues to the equatorial Kerr–Newman black hole," *Commun. Phys.* **3**(1), 120 (2020).
9. Y. Rosenberg, "Optical analogues of black-hole horizons," *Phil. Trans. R. Soc. A* **378**(2177), 20190232 (2020).
10. J. Zhang, K. F. MacDonald, and N. I. Zheludev, "Controlling light-with-light without nonlinearity," *Light Sci. Appl.* **1**(7), e18 (2012).
11. W. W. Salisbury, "Absorbent body for electromagnetic waves," Patent No. US 2599944(A) (10 June 1952).
12. H.-T. Chen, "Interference theory of metamaterial perfect absorbers," *Opt. Express* **20**(7), 7165–7172 (2012).
13. M. A. Kats and F. Capasso, "Optical absorbers based on strong interference in ultra-thin films," *Laser Photonics Rev.* **10**(5), 735–749 (2016).
14. L. Wu et al., "Ultra-broadband and wide-angle plasmonic absorber based on all-dielectric gallium arsenide pyramid nanostructure for full solar radiation spectrum range," *Int. J. Therm. Sci.* **201**, 109043 (2024).
15. Y. Cheng et al., "Terahertz pseudo-waveform-selective metasurface absorber based on a square-patch structure loaded with linear circuit components," *Adv. Photonics Res.* **5**(8), 2300303 (2024).
16. E. Plum et al., "Controlling the optical response of 2D matter in standing waves," *ACS Photonics* **4**(12), 3000–3011 (2017).

17. D. G. Baranov et al., "Coherent perfect absorbers: linear control of light with light," *Nat. Rev. Mater.* **2**(12), 17064 (2017).
18. C. Hägglund, S. P. Apell, and B. Kasemo, "Maximized optical absorption in ultrathin films and its application to plasmon-based two-dimensional photovoltaics," *Nano Lett.* **10**(8), 3135–3141 (2010).
19. S. Thongrattanasiri, F. H. L. Koppens, and F. J. García de Abajo, "Complete optical absorption in periodically patterned graphene," *Phys. Rev. Lett.* **108**(4), 047401 (2012).
20. S. M. Rao et al., "Coherent control of light interaction with graphene," *Opt. Lett.* **39**(18), 5345–5374 (2014).
21. A. Goodarzi, M. Ghanaatshoar, and M. Mozafari, "All-optical fiber optic coherent amplifier," *Sci. Rep.* **8**(1), 15340 (2018).
22. A. N. Vetlugin et al., "Anti-Hong–Ou–Mandel interference by coherent perfect absorption of entangled photons," *New J. Phys.* **24**(12), 122001 (2022).
23. A. N. Vetlugin et al., "Photon number resolution without optical mode multiplication," *Nanophotonics* **12**(3), 505–519 (2023).
24. C. Yan et al., "Coherent perfect absorption of electromagnetic wave in subwavelength structures," *Opt. Laser Technol.* **101**, 499–506 (2018).
25. P. T. Landsberg and G. Tonge, "Thermodynamic energy conversion efficiencies," *J. Appl. Phys.* **51**(7), R1–R20 (1980).
26. T. Roger et al., "Coherent perfect absorption in deeply subwavelength films in the single-photon regime," *Nat. Commun.* **6**(1), 7031 (2015).
27. C. M. X. Altuzarra et al., "Coherent perfect absorption in metamaterials with entangled photons," *ACS Photonics* **4**(9), 2124–2128 (2017).
28. V. Nalla et al., "100 THz optical switching with plasmonic metamaterial," *presented at the CLEO/Europe-EQEC 2015*, Munich, Germany (2015).
29. S. Yanikgonul et al., "Phase stabilization of a coherent fiber network by single-photon counting," *Opt. Lett.* **45**(10), 2740–2743 (2020).
30. A. Xomalis et al., "Fibre-optic metadevice for all-optical signal modulation based on coherent absorption," *Nat. Commun.* **9**(1), 182 (2018).
31. A. N. Vetlugin et al., "Deterministic generation of entanglement in a quantum network by coherent absorption of a single photon," *Phys. Rev. A* **106**(1), 012402 (2022).
32. M. Papaioannou, E. Plum, and N. I. Zheludev, "All-optical pattern recognition and image processing on a metamaterial beam splitter," *ACS Photonics* **4**(2), 217–222 (2017).
33. H. Mashaal et al., "First direct measurement of the spatial coherence of sunlight," *Opt. Lett.* **37**(17), 3516–3518 (2012).
34. M. V. Berry, "The adiabatic phase and pancharatnam's phase for polarized light," *J. Mod. Opt.* **34**(11), 1401–1407 (1987).
35. M. Lanoy et al., "Broadband coherent perfect absorption of acoustic waves with bubble metascreens," *Appl. Phys. Lett.* **113**(17), 171907 (2018).
36. C. Meng et al., "Acoustic coherent perfect absorbers as sensitive null detectors," *Sci. Rep.* **7**(1), 43574 (2017).
37. P. Wei et al., "Symmetrical and anti-symmetrical coherent perfect absorption for acoustic waves," *Appl. Phys. Lett.* **104**(12), 121902 (2014).
38. P. B. Johnson and R. W. Christy, "Optical constants of transition metals: Ti, V, Cr, Mn, Fe, Co, Ni, and Pd," *Phys. Rev. B* **9**(12), 5056–5070 (1974).
39. J. Pflüger et al., "Dielectric properties of TiC_x, TiN_x, VC_x, and VN_x from 1.5 to 40 ev determined by electron-energy-loss spectroscopy," *Phys. Rev. B* **30**(3), 1155–1163 (1984).
40. A. B. Djurišić and E. H. Li, "Optical properties of graphite," *J. Appl. Phys.* **85**(10), 7404–7410 (1999).
41. M. R. Querry, "Optical constants," Contractor Report CRDC-CR-85034 (1985).
42. A. Banerjee et al., "Optical properties of refractory metal based thin films," *Opt. Mater. Express* **8**(8), 2072–2088 (2018).
43. M. Pu et al., "Ultrathin broadband nearly perfect absorber with symmetrical coherent illumination," *Opt. Express* **20**(3), 2246–2254 (2012).
44. F. A. Jenkins and H. E. White, *Fundamentals of Optics*, 4th ed., McGraw-Hill (1976).

Eric Plum is a principal research fellow at the Optoelectronics Research Centre (ORC), University of Southampton, UK and a Marconi Society Paul Baron Young Scholar. His research interests include reconfigurable metamaterials, coherent absorption, and chirality. He joined the ORC after undergraduate studies at RWTH Aachen (Germany), University of Southampton (UK) and as a Fulbright Scholar at New Mexico Tech (USA).

Anton N. Vetlugin is a senior research fellow at the Centre for Disruptive Photonic Technologies at Nanyang Technological University in Singapore. His research interests focus on coherent phenomena in classical and quantum optics and problems of light detection.

Baurzhan Salimzhanov is a PhD candidate at the Optoelectronics Research Centre, University of Southampton, UK. His research focuses on light-matter interactions. Before joining Southampton, he completed his master's degree in material science and engineering at the Ulsan National Institute of Science and Technology (UNIST), where he worked on photovoltaics.

Nina Vaidya is an assistant professor at the University of Southampton, UK, after postdoctoral fellowship at Caltech, USA. She completed undergraduate study at the University of Cambridge, UK and PhD at Stanford University, USA. She specializes in optics, optoelectronics, and material design. Her notable innovations include AGILE (Axially Graded Index LEns) concentrators, 3D printed optics, and her work at Caltech's Space-Based-Solar-Power project with successful demo results from space in 2024.